

Sagnac Interferometer for Gravitational-Wave Detection

Ke-Xun Sun, M. M. Fejer, Eric Gustafson, and Robert L. Byer

Edward L. Ginzton Laboratory, Stanford University, Stanford, California 94305-4085

(Received 21 August 1995)

We have investigated a zero-area Sagnac interferometer as a broad band gravitational-wave detector. Frequency response measurements of a laboratory-scale interferometer are in excellent agreement with theory. The measured contrast ratio, 0.996, is insensitive to induced birefringence, laser-frequency variation, arm imbalance, and dc mirror displacement. A near shot-noise-limited phase sensitivity of 3×10^{-9} rad/ $\sqrt{\text{Hz}}$ was measured at the interferometer's maximum sensitivity frequency, 90.9 MHz.

PACS numbers: 04.80.Nn, 07.60.Ly, 42.25.Hz, 42.62.-b

The progress in gravitational-wave receivers over the past three decades [1–8] has led to the initiation of the Laser Interferometer Gravitational-Wave Observatory (LIGO) [4], which will consist of two 4-km Michelson-Fabry-Pérot interferometers. The initial LIGO interferometers are expected to meet their phase and strain sensitivity requirements with ~ 100 W of laser power on the beam splitter. However, an advanced interferometer will require several kilowatts of laser power at the beam splitter and will be difficult to build using existing technology. An advanced LIGO interferometer must address the issues of laser noise, interferometer fringe-contrast ratio, thermally induced figure changes, birefringence, and depolarization. We describe here a zero-area Sagnac interferometer with the potential to meet the advanced LIGO sensitivity requirements.

The Sagnac interferometer [9,10], invented in 1913 for rotation sensing, is an interferometer in which waves traveling in opposite directions experience common optical paths. The differential phase $\Delta\phi = \phi_{\text{ccw}} - \phi_{\text{cw}}$, where ϕ_{ccw} and ϕ_{cw} are the phases of counterclockwise waves, is detected to obtain dynamical information about the optical paths. The gyroscope interferometer is a ring that encloses an area as shown in Fig. 1(a). A considerable body of knowledge regarding the sensitivity limits of Sagnac interferometers is available due to development of advanced fiber-optic gyroscopes [11,12]. In 1986, Weiss proposed an open-area Sagnac interferometer for gravitational-wave detection [13]. In 1982, Drever proposed a “multireflection Michelson interferometer,” a ring cavity device whose resonant recycling enhances sensitivity for narrow band detection of periodic gravitational-wave signals [3]. Recently, a prototype gravitomagnetic field sensor incorporating a Sagnac ring was described in [14].

We have analyzed and experimentally investigated the zero-area Sagnac interferometer shown in Fig. 1(b) as a topology for an advanced gravitational-wave receiver. This zero-area interferometer, modified from a conventional Sagnac by area cancellation, remains sensitive to time-dependent displacements in the arms but insensitive to rotation. It enjoys several advantages over a Michelson interferometer as an advanced interferometer for LIGO. Specifically, this interferometer is insensitive to laser-

frequency variation, mirror displacement at dc, thermally induced birefringence, and reflectivity imbalance in the arms, allowing a simplified control system and reduced optical tolerance requirements. The peak response of the Sagnac interferometer lies in the central part of the gravitational-wave frequency band of astrophysical interest, and is greater than that of a Michelson interferometer with the same storage time and power on the beam splitter.

In a common-path interferometer only a nonreciprocal or time-dependent element, such as a Faraday rotator or an asymmetrically placed optical phase modulator, affects the fringe at the beam splitter. A gravitational wave, produc-

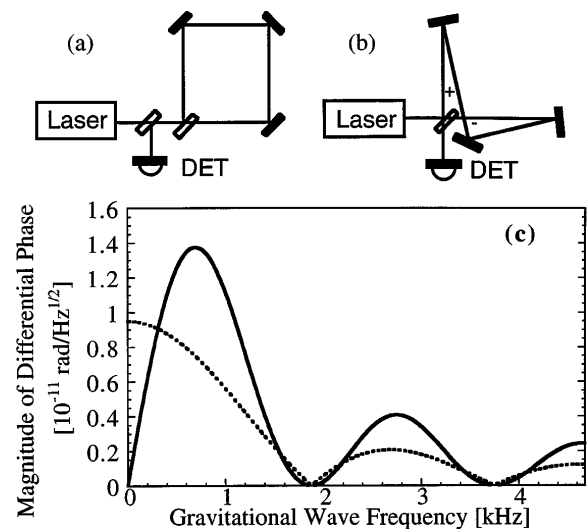


FIG. 1. (a) Conventional Sagnac interferometer. (b) Zero-area Sagnac interferometer for displacement sensing with a geometry that meets LIGO requirements. (c) Theoretically calculated differential phase generated by a gravitational wave with strain $h_g \sim 10^{-23}/\sqrt{\text{Hz}}$, in a 20-bounce (bounce number $N = 20$) delay line, 4-km arm-length, zero-area Sagnac interferometer illuminated with a 1064-nm laser. The Michelson interferometer response (dashed line) is shown for comparison. The Sagnac response peaks at 690 Hz and has a 3-dB bandwidth of 220–1250 Hz. Assuming a 75% system efficiency, detection of a differential phase at the shot noise limit of 10^{-11} rad/ $\sqrt{\text{Hz}}$, requires ~ 5 kW of laser power on the beam splitter. At this power level, the shot-noise-limited strain sensitivity falls to $10^{-22}/\sqrt{\text{Hz}}$ at $f_g \approx 32$ Hz, a frequency at which seismic and thermal displacement noise will dominate.

ing space-time tidal fluctuations in the optical path, also gives rise to an interferometer response. Assuming that the gravitational wave is normally incident onto the detector plane with “+” polarization whose base tensor components are along the interferometer arms, then the strains along each interferometer arm are out of phase by 180° , and, consequently, clockwise and counterclockwise waves experience time-dependent phase shifts obeying $\phi_{cw} = -\phi_{ccw}$. The differential phase of the two counterpropagating waves is given by $\Delta\phi = 2\phi_{ccw}$, where ϕ_{ccw} is determined by integration along the Sagnac path:

$$\begin{aligned} \phi_{ccw} &= 2\pi f_l \left[\int_{t-2\tau_s}^{t-\tau_s} \left(\frac{h_g}{2}\right) e^{i2\pi f_g t} dt \right. \\ &\quad \left. - \int_{t-\tau_s}^t \left(\frac{h_g}{2}\right) e^{i2\pi f_g t} dt \right] \\ &= (2f_l h_g / i f_g) \sin^2(\pi \tau_s f_g) e^{i2\pi f_g (t-\tau_s)}, \end{aligned} \quad (1)$$

where f_l is the laser frequency, τ_s is the single-arm storage time, and h_g and f_g are the gravitational-wave strain and frequency, respectively. The absolute magnitude of the differential phase is

$$|\Delta\phi| = 4f_l h_g f_g^{-1} \sin^2(\pi \tau_s f_g). \quad (2)$$

The absolute magnitude of the differential phase for a delay-line Michelson interferometer can be calculated similarly [8],

$$|\Delta\phi_m| = 2f_l h_g f_g^{-1} |\sin(\pi \tau_s f_g)|. \quad (3)$$

For both the Sagnac and Michelson interferometers, the single-arm storage time τ_s is defined as $\tau_s = 2NL/c$, where L is their arm length, N is the number of bounces on the end mirror of the delay line, and c is the speed of light.

Figure 1(c) shows the response functions for 4-km 20-bounce ($N = 20$) LIGO-scale interferometers illuminated with a 1064-nm Nd:YAG laser. The Michelson interferometer has its peak response at dc and subpeaks at frequencies determined by the transcendental equation $x = \tan x$, where $x = \pi \tau_s f_g$. The Sagnac interferometer has its peak and subpeak responses at frequencies determined by $2x = \tan x$. The first and highest peak occurs at $f_{g,\max} = 0.37/\tau_s = 0.74/\tau_{\text{loop}}$, where τ_{loop} is the loop time of the Sagnac interferometer. Proper setting of τ_s allows the peak response frequency to be tuned to the gravitational-wave band of interest; for this example $f_{g,\max} \approx 690$ Hz. The first peak of the Sagnac-interferometer response has a 3-dB bandwidth of $0.54/\tau_s$, which for this example extends from 220 to 1250 Hz. The peak response of the Sagnac interferometer is higher than that of the Michelson interferometer due to the phase change accumulated in passing through both arms before interfering at the beam splitter.

Unlike a Michelson interferometer, the Sagnac interferometer has no response at zero frequency. Therefore, the static length of the interferometer arm does not need to be controlled. The interferometer is insensitive to slow length changes due to mirror movements caused by seis-

mic vibrations, gravity gradients, and thermal effects—a feature that offers significant advantages in the design and operation of the advanced interferometer for LIGO. The effect of the reduced low-frequency responsivity of the Sagnac topology on the sensitivity for gravitational-wave detection depends on the relative magnitudes of phase and displacement noise spectra. Under typical assumptions for advanced LIGO, the sensitivity of a Sagnac interferometer with a storage time of 0.53 ms (20 bounces in a 4-km arm) would fall below that of a delay-line Michelson with the same storage time over the frequency range 15 to 300 Hz, and rise above that of a Michelson at frequencies higher than 300 Hz. For a storage time of 2.1 ms, the Sagnac would have sensitivity equal to that of a Michelson from 15 to 80 Hz, and greater sensitivity at frequencies above 80 Hz.

Figure 2 shows a schematic of our laboratory-scale Sagnac interferometer. We illuminate the interferometer with a 300-mW (Lightware Electronics model 122) diode-laser-pumped Nd:YAG laser. The laser beam passes through a quarter-wave plate and a half-wave plate and then is incident on the Sagnac beam splitter. The beam splitter is 50% reflective for the S polarization and 1% for the P polarization. The Sagnac optical path encloses zero area to avoid rotation sensitivity and to provide a geometry compatible with the LIGO vacuum system. An asymmetrically placed electro-optic (EO) phase modulator (NewFocus model 4004) provides phase modulation for S -polarized light to simulate a gravitational-wave signal. An optional quarter-wave plate inside the interferometer is used to determine the sensitivity of the interferometer to birefringence. The dark-port output is incident on a scanning confocal interferometer for optical spectral analysis, on dc detectors for power measurements, and on an RF detector for RF spectral analysis.

The frequency response of a Sagnac interferometer to a spatially lumped phase modulation is derived from Eq. (1) by replacing the integrand with δ functions, and expanding the field in a series of Bessel functions. With a 50% beam splitter, the first-sideband response function

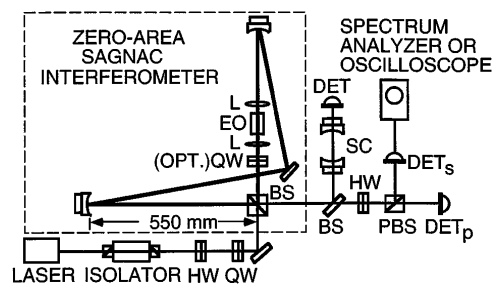


FIG. 2. Schematic of experimental setup for the Sagnac interferometer. Bold line: Sagnac loop, EO: electro-optic modulator, BS: beam splitter, PBS: polarizing beam splitter, HW: half-wave plate, QW: quarter-wave plate, L: lens, SC: scanning confocal optical spectrum analyzer. The light source is a 300-mW Nd:YAG laser.

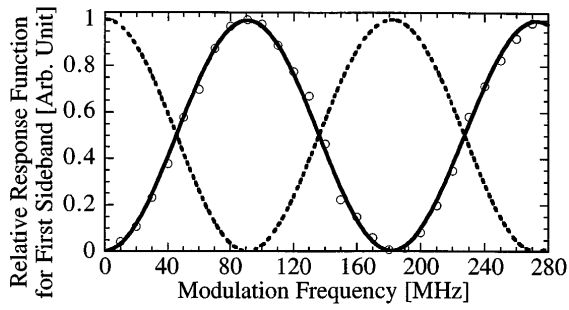


FIG. 3. Theoretical transfer function (solid line) and experimental data (circles) for the first-order Bessel sideband of the Sagnac interferometer. Transfer function of a Michelson interferometer with an electro-optic modulator is shown by the dashed line for comparison.

normalized to the input power is given by

$$T_{1,s}(f_{\text{mod}}) = \frac{P_1}{P_{\text{in}}} = J_1^2(m) \sin^2[\pi f_{\text{mod}}(\tau_{\text{ccw}} - \tau_{\text{cw}})] \approx \frac{1}{4} m^2 \sin^2[\pi f_{\text{mod}}(\tau_{\text{ccw}} - \tau_{\text{cw}})], \quad (4)$$

where P_{in} is the input power, P_1 is the power in the first sideband, J_1 is the first-order Bessel function, m is the phase modulation depth in radians, f_{mod} is the modulation frequency, and τ_{ccw} and τ_{cw} are the time separations between the modulator position and the beam splitter for the counterclockwise and clockwise beams, respectively. The approximate form of Eq. (4) holds for small modulation, $|m| \ll 1$. The peak response occurs at a modulation frequency $f_{\text{max}} = 2/|\tau_{\text{ccw}} - \tau_{\text{cw}}|$. If the modulator is placed at the symmetry point, there is no signal. The tabletop experiment allows counterclockwise and clockwise optical path lengths from the EO to the interferometer beam splitter to be 330 and 1979 mm, respectively, and hence the peak sensitivity is at a 90.9-MHz modulation frequency.

For comparison a Michelson interferometer with an in-arm, double-passed, lumped EO, has a corresponding response function given by

$$T_{1,m}(f_{\text{mod}}) = \frac{1}{4} J_1^2(m_{\text{eqv}}) \approx \frac{1}{4} m^2 \cos^2[2\pi f_{\text{mod}} \tau_M], \quad (5)$$

where the equivalent modulation depth $m_{\text{eqv}} = 2m \cos(2\pi f_{\text{mod}} \tau_M)$ and τ_M is the time separation between the end mirror of the Michelson interferometer and the EO. The approximate form of Eq. (5) is valid for $|m| \ll 1$. For $\tau_M = |\tau_{\text{ccw}} - \tau_{\text{cw}}|/2$, the Michelson response is phase shifted by 90° with respect to that of the Sagnac.

Figure 3 shows the relative response of the Sagnac interferometer as a function of the modulation frequency, demonstrating an excellent agreement between theory and experiment. For this measurement, we varied the EO modulation frequency from 10 to 270 MHz and calibrated the EO modulation depth at each frequency. The modulation depths were limited to less than 0.47% to remain in the linear regime. The optical spectrum

analyzer was used to measure the power of the first Bessel sideband.

The shot-noise-limited phase sensitivity of a Sagnac interferometer, which equivalent to a Michelson interferometer, assuming an optimal homodyne detection scheme at the dark port and coherent states for all inputs, is

$$|\Delta\phi| \approx \sqrt{2(P_{\text{LO}} + P_{\text{min}})2\pi\hbar f_l / P_{\text{LO}} P_{\text{in}} \eta C^2}, \quad (6)$$

where P_{LO} is the local oscillator power, P_{min} is the leakage power from the dark port, \hbar is the reduced Planck constant, P_{in} is the interferometer input power, η is the quantum efficiency of the photodetector, and the contrast ratio $C \equiv (P_{\text{max}} - P_{\text{min}})/(P_{\text{max}} + P_{\text{min}})$, where P_{max} is the maximum power out of the bright port. For less-than-unity contrast ratio, the power incident onto the detector is given by $P + P_{\text{min}}$. A near-unity contrast ratio is desirable in an interferometer for two reasons; first, the phase sensitivity reaches the quantum limit only if the contrast ratio approaches unity; second, the photodetector saturates if illuminated with too much leakage power.

Experimentally, the power directly out of the dark port, P_{min} , was measured to be 27 dB below that of the bright port, P_{max} , giving a contrast ratio of 0.996. The dark-port power measured after the scanning confocal interferometer, which spatially filters the dark-port output, was 30 dB below the bright-port output, giving a contrast ratio of 0.998. This high contrast ratio was obtained despite the phase modulator and two lenses that were placed asymmetrically in one arm of the interferometer.

The dark and bright fringes were nearly constant and the contrast ratio varied by less than 0.002, when one of the arm-end mirrors was driven at 20 Hz over a distance of a full optical wavelength, for which two periods of interference fringes would occur in a Michelson interferometer. The insensitivity of the dark fringe of the Sagnac interferometer to mirror displacements near dc allowed our experiments to be done without active stabilization, resulting in a substantially reduced control problem compared to that of a Michelson interferometer.

We inserted a quarter-wave plate into one arm of the Sagnac interferometer to simulate the impact of thermally induced birefringence in optical elements under the high-power illumination expected for an advanced interferometer. Experimentally, for 0° to 45° rotation of the quarter-wave plate, the contrast ratio of the interferometer, as expected, remained near unity, varying less than 0.004. The small variation was mainly due to the nonuniformity of the inserted wave plate. By comparison, the contrast ratio for a Michelson interferometer approaches zero for quarter-wave retardation in one arm.

We inserted neutral-density filters into one arm of the Sagnac interferometer to simulate the effect of in-arm attenuation. The contrast ratio, as expected, was found to be near unity (variation less than 0.002) over greater than 10 dB of attenuation, for which the contrast ratio for a Michelson interferometer would degrade to 0.58. This re-

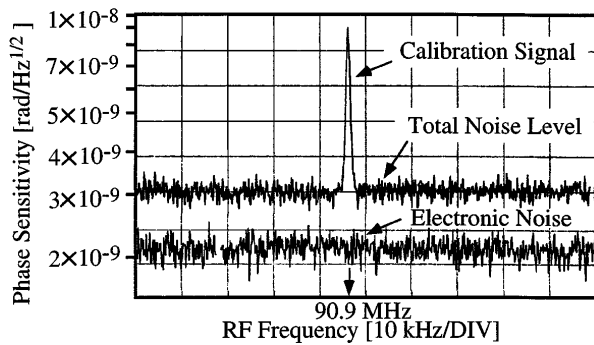


FIG. 4. Near-shot-noise-limited phase-sensitivity measurement at 90.9 MHz for the Sagnac interferometer. The calibration signal, the total noise (shot noise plus electronic noise), and the electronic noise levels are shown. Phase sensitivity, 3×10^{-9} rad/ $\sqrt{\text{Hz}}$, within 3 dB of shot-noise limit.

sult shows that a Sagnac interferometer allows considerable tolerance for matching the mirror reflectivities.

The Sagnac interferometer, due to its equal optical paths, is a white light interferometer whose null point should be insensitive to laser frequency. We demonstrated that the contrast ratio is independent of laser frequency by tuning the Nd:YAG laser more than 30 GHz, and observing no change in the contrast ratio. This feature allows the laser to be operated in the multi-axial or even superfluorescent modes, as is used in fiber-optic gyroscopes. The use of broad band radiation simplifies the engineering of the high-power laser, and reduces the sensitivity to scattered light at the detector to that generated within one coherence length of the midpoint of the loop [12].

Figure 4 shows the result of the phase sensitivity measurement of the Sagnac interferometer at the peak response frequency of 90.9 MHz. Wave plates at the input of the interferometer produced a small *P*-polarized component in the laser beam to act as a local oscillator (LO) for heterodyne detection. The *P*-polarized light was mostly transmitted through the interferometer since the beam splitter was 99% transmissive for *P* polarization. The polarizations of the *P*- and *S*-polarized components, i.e., the LO and the signal, were rotated at the interferometer output port by a half-wave plate, so that both *S* and *P* polarizations thereafter contained the LO and the signal. A polarizing beam splitter then separated the two polarizations. The LO and signal fields now in *P* polarization were mixed for heterodyne detection in this experiment. The LO and signal in *S* polarization can be further used for balanced detection in the future. This scheme allows the local oscillator power to be adjusted by simply rotating a wave plate prior to the Sagnac interferometer. In the present experiment, the local oscillator was optimized at 6 mW, which set the total noise 3 dB above

the electronic noise level. The transmission of the local oscillator through the Sagnac interferometer is frequency independent and therefore laser frequency noise does not affect the signal extraction, in contrast to the behavior of an asymmetric-arm-based signal extraction scheme for a Michelson interferometer [15]. With the 90.9-MHz signal, we could use a dc LO. To measure a low-frequency gravitational-wave signal, an LO with a frequency above the amplitude noise corner of the laser would be used.

The phase sensitivity was 3×10^{-9} rad/ $\sqrt{\text{Hz}}$ at 90.9 MHz. The phase noise measurement was made without having to control the absolute length of the interferometer. The sensitivity exceeds that of other benchtop experiments [16], demonstrating a signal extraction scheme that retains the advantages of the common path of the Sagnac interferometer, and allows optimization of the LO power at the detector.

To summarize, we have analyzed and experimentally investigated the zero-area Sagnac interferometer as a potential advanced LIGO interferometer. In the future, we plan to investigate delay line, Fabry-Pérot, and recycling schemes for the Sagnac interferometer. We are developing a vacuum-isolated suspended-mass Sagnac interferometer with extended storage time to carry out phase measurements at lower frequencies.

This research was supported by National Science Foundation (Grant No. NSF PHY 92-15157).

- [1] J. Weber, Phys. Rev. Lett. **22**, 1320 (1969).
- [2] R. Weiss, MIT Res. Lab. Electron. Q. Rep. **105**, 54 (1972).
- [3] R. W. P. Drever, in *Gravitational Radiation*, edited by N. Deruelle and T. Piran (North-Holland, Amsterdam, 1983).
- [4] K. S. Thorne, in *300 Years of Gravitation*, edited by S. W. Hawking and W. Israel (Cambridge Univ. Press, Cambridge, 1987).
- [5] K. A. Strain and B. Meers, Phys. Rev. Lett. **66**, 1391 (1991).
- [6] A. Abramovici *et al.*, Science **256**, 5055 (1992).
- [7] W. Johnson and S. Merkowitz, Phys. Rev. Lett. **70**, 2367 (1993).
- [8] P. Saulson, *Fundamentals of Interferometric Gravitational Wave Detectors* (World Scientific, Singapore, 1994).
- [9] G. Sagnac, C. R. Acad. Sci. **95**, 1410 (1913).
- [10] E. J. Post, Rev. Mod. Phys. **39**, 475 (1967).
- [11] *Fiber-Optic Rotation Sensors*, edited by S. Ezekiel and H. J. Arditty (Springer-Verlag, Berlin, 1982).
- [12] H. Lefevre, *The Fiber-Optic Gyroscope* (Artech House, Boston, 1993).
- [13] R. Weiss, in NSF Proposal, 1987.
- [14] N. Sampas, Ph.D. thesis, University of Colorado, 1990.
- [15] M. W. Regehr, F. J. Raab, and S. E. Whitcomb, Opt. Lett. **20**, 1507 (1995).
- [16] A. J. Stevenson, M. B. Gray, H.-A. Bachor, and D. E. McLelland, Appl. Opt. **32**, 3481 (1993).